

# The First Billion Years project: Finding Infant Globular Clusters at $z = 6$

Frederika Phipps<sup>1\*</sup>, Sadegh Khochfar<sup>1</sup>, Anna Lisa Varri<sup>1,2</sup> and Claudio Dalla Vecchia<sup>3,4</sup>

<sup>1</sup>*Institute for Astronomy, University of Edinburgh, Royal Observatory, Edinburgh EH9 3HJ*

<sup>2</sup>*Department of Astronomy, Graduate School of Science, The University of Tokyo, 7-3-1 Hongo, Bunkyo-ku, Tokyo, 113-0033, Japan*

<sup>3</sup>*Instituto de Astrofísica de Canarias, E-38205 La Laguna, Tenerife, Spain*

<sup>4</sup>*Universidad de La Laguna, Dpto Astrofísica, E-38206 La Laguna, Tenerife, Spain*

Accepted XXX. Received YYY; in original form ZZZ

## ABSTRACT

We explore a suite of high-resolution cosmological simulations from the First Billion Years (FiBY) project at  $z \geq 6$  to identify low-mass stellar systems, with a particular focus on globular clusters (GCs). Within the demographics of substructures found in the simulations, two distinct groups of objects emerge. We associate the first group, which appear to have a high baryon fraction ( $f_b \geq 0.95$ ), with infant GC candidates. The second group exhibit a high stellar fraction ( $f_* \geq 0.95$ ) and show a resemblance to ultra-faint dwarf galaxies. The infant GC candidates are characterised by a stellar content similar to the one observed in present-day GCs, but they still contain a high gas fraction ( $f_{\text{gas}} \sim 0.95$ ) and a relatively low amount of dark matter. They are very compact systems, with high stellar mass densities and sizes which are consistent with recent estimates based on the first observations of possible proto-GCs at high redshifts. Such infant GCs appear to be more massive and more abundant in massive host galaxies, indicating that the assembly of galaxies via mergers may play an important role in shaping up several GC-host scaling relations. Specifically, we express the relation between the mass of the most massive infant GC and its host stellar mass as  $\log(M_{\text{cl}}) = (0.31 \pm 0.15) \log(M_{*,\text{gal}}) + (4.17 \pm 1.06)$ . Finally, we assess that the present-day GC mass – halo mass relation offers a satisfactory description of the behaviour of our infant GC candidates at high redshift, suggesting that such a relation may be set at formation.

**Key words:** galaxies: formation – galaxies: high-redshift – globular clusters: general

## 1 INTRODUCTION

In the rich context of contemporary research in astrophysics, the formation and evolution of galaxies is one of the key problems to still be fully understood. The currently favoured standard paradigm for the formation of structures in the universe is the  $\Lambda$ CDM model. Within this model, potential wells generated by dark matter haloes drive the gravitational collapse of baryons. Once dense enough, self-gravity starts taking over and gas clouds collapse further to form stars, stellar clusters and galaxies. As baryons collapse dark matter haloes continue to grow via accretion and mergers which lead to the hierarchical growth of cosmic structures. While this general picture is now consolidated, important details still remain to be understood. Specifically, thanks to the gradual increase of the numerical resolution of state-of-the-art cosmological simulations, the behaviour of key as-

trophysical processes on progressively smaller scales can finally be assessed. Such a progress creates the opportunity to attack a number of long-standing questions related to the formation and evolution of low-mass stellar systems in the early universe. A particularly deep-rooted problem concerns the distinction between the formation of star clusters and proto-galaxies, especially when both classes of stellar systems are of similar stellar mass. Given the wealth of data expected from current and forthcoming observational facilities focused on the exploration of the high-redshift Universe, it is imperative for improving our understanding of galaxy evolution to be able to link high-redshift objects with their local descendants.

Globular star clusters are among the most ancient gravitationally bound stellar systems. They are ubiquitous in the way that they can be found around any type of galaxy from dwarf to elliptical (e.g., see Harris & Racine 1979; Harris 2016). They are massive ( $10^4 - 10^7 M_{\odot}$ ), compact, approximately spherical, dense star clusters (e.g., see Harris 1996;

\* E-mail: phipps@roe.ac.uk

Renaud 2018). Their stellar populations are extremely old in age ( $\sim 11.5 - 12.5$  Gyr) and therefore it is believed that they formed during or just after the epoch of reionisation (e.g., see Ricotti 2002; Katz & Ricotti 2014). Hence, for this reason, studying these systems at high redshift can not only give insight into the processes and environments that governed star formation at that time, but they can also represent valuable probes of the reionisation epoch itself (e.g., see Paardekooper et al. 2013; Boylan-Kolchin 2018). Investigating the formation of GCs also allows one to constrain the dynamical and chemical conditions in forming galaxies, and, through comparisons with local Universe observations, this can impart constraints on models relating to, for example, merger histories (Kruijssen et al. 2019; Renaud 2018). However, in order to use GCs as a tool to probe the formation and evolution of galaxies, one needs to discern them from proto-galaxies and other bound stellar systems. There are a number of key questions and observational features concerning GCs that still need to be explained. These include the physical origin of the observed multiple stellar populations (Lardo et al. 2011; Piotto et al. 2015; Milone et al. 2017; Bastian & Lardo 2018), the colour bi-modality (Larsen et al. 2001; Peng et al. 2006; Renaud et al. 2017), the split in the age-metallicity plane (Forbes & Bridges 2010; Leaman et al. 2013; Recio-Blanco 2018), the tight correlations between GC system mass and host galaxy halo mass (Spitler & Forbes 2009; Harris et al. 2015, 2017; Forbes et al. 2018b), to name just a few. For each of these interesting aspects of GCs, it is unclear whether these features emerge due to their formation or are a result of the subsequent evolution they undergo, which makes identifying them at high-redshifts challenging.

The environmental conditions required and the exact nature of the formation of GCs are still unknown. However, many theories about formation scenarios of globulars have been put forward. Peebles & Dicke (1968) proposed that GCs formed before the first galaxies in low metallicity environments. Whilst plausible, this theory would not result in a bimodality among the clusters. Rosenblatt et al. (1988) amended the Peebles-Dicke scenario by assuming that pregalactic globulars formed within cold dark matter halos, but only those formed in high- $\sigma$  fluctuations would survive to present day. Schweizer (1987) and Ashman & Zepf (1992) suggested a two-step formation channel for the formation of GCs which would account for the observed colour bimodality. They state that the blue (metal-poor) GCs form via the scenario proposed by Peebles & Dicke. The red (metal-rich) GCs are then formed when star formation is triggered during mergers. Yet, unfortunately, this would likely result in a unimodal distribution rather than a bimodal one. Forbes et al. (1997) suggested that metal-poor clusters form during the collapse of the proto-galaxies. The more metal-rich GCs would then form during the assembly of galactic disks, as a result of local collapse and fragmentation of enriched material in the interstellar medium. Another crucial aspect that any formation theory of GCs needs to address concerns their expected amount of dark matter (DM) content, both at formation as well as at their present-day conditions. Were these objects formed by gravitational instabilities driven purely by baryons without the need for dark matter? Or were they formed within a local potential minimum generated by dark matter? Is such a dark matter halo entirely lacking today, as possibly due to the interplay between external (e.g. see

Moore 1996; Saitoh et al. 2006; Creasey et al. 2019) and internal dynamical processes (e.g. see Bromm & Clarke 2002; Mashchenko & Sills 2005; Hurst & Zentner 2019) as well as feedback processes (Pontzen & Governato 2012; Davis et al. 2014)? Or are some remnants still preserved in the peripheries of present-day GCs (e.g., see Heggie & Hut 1996; Baumgardt et al. 2009; Lane et al. 2010; Conroy et al. 2011; Ibata et al. 2013; Penarrubia et al. 2017)?

On the one hand, in order to address these questions in the local Universe, detailed astrometric and spectroscopic observations of member stars in the extreme peripheries of GCs are required and the structural and kinematic properties of these stellar systems in their very outer regions must be explored. These empirical assessments have become possible only recently, thanks to the on-going mission Gaia (Gaia Collaboration et al. 2018). On the other hand, to directly determine the exact formation channel for GCs via observations in the early Universe it is still extremely challenging, as due to the high redshift at which they are believed to have formed. Whilst there is growing evidence that proto-globular-like objects have already been detected (Vanzella et al. 2017; Elmegreen & Elmegreen 2017; Bouwens et al. 2017; Kikuchi et al. 2019; Vanzella et al. 2019), these observations do not yet provide the depth and detail required to empirically assess the phenomenological implications of the different formation scenarios. However, as we enter the era of the James Webb Space Telescope (JWST) and the Extremely Large Telescopes (ELTs), the opportunity to directly observe massive infant star clusters may soon be on the horizon (Katz & Ricotti 2013; Renzini 2017; Forbes et al. 2018a; Pozzetti et al. 2019).

Numerical simulations offer an alternative view to study the formation of low-mass stellar systems and to test current theoretical models. Over recent years, the resolution of cosmological simulations has increased greatly and the models describing the underlying physics have been significantly improved. After some first numerical investigations conducted either in local (e.g. Nakasato et al. 2000; Bate et al. 2003) or cosmological settings (e.g. see Kravtsov & Gnedin 2005; Prieto & Gnedin 2008), several groups now use a variety of simulation suites to study the formation of GCs (e.g. Ishiyama et al. 2013; Rieder et al. 2013; Ricotti et al. 2016; Kim et al. 2018; Carlberg 2018; Reina-Campos et al. 2019; Li & Gnedin 2019; Ma et al. 2019). Some of these studies rely on present-day observational criteria to identify and study globular-like clusters. One recent example is the study conducted by Halbesma et al. (2019) to identify GC candidates within the Auriga simulations. They were interested in assessing whether the galaxy and star formation models implemented in their simulations were able to also reproduce a realistic GC population. They identified GC candidates by selecting star particles which had an age older than 10 Gyr, which would imply that all stars present in their simulations at  $z \geq 6$  are GC members. One local observational property of GC systems that has been used to identify globulars at high- $z$  in simulations is the GC system - halo mass relation. In their work, Creasey et al. (2019) assumed that a GC formed within any halo which had a virial mass  $\geq 10^8 M_{\odot}$ . Other approaches include looking at gravitationally bound star clusters of a given mass in zoom-simulations throughout cosmic time (e.g. Ma et al. 2019). Whilst such approaches are effective in selecting promising

candidates, it could lead to a bias in results and any predictions that are made because GCs are likely to dynamically evolve over time, with a significant impact both on their total mass, individual mass function as well as their detailed phase space structure (for an overview see, e.g. Elson et al. 1987; Meylan & Heggie 1997; Heggie & Hut 2003, and, more recently, Portegies Zwart et al. 2010; Gratton et al. 2012; Kruijssen 2014; Bastian & Lardo 2018; Renaud 2018). Also, it is not evident that all bound objects in a given mass range can be uniformly and reliably classified as GCs. Ideally, one would like to combine different criteria to produce a selection for infant GC candidates that matches physical constraints on them, both in the early and local Universe.

In this work, we explore a suite of high-resolution cosmological simulations from the First Billion Years (FiBY) project at  $z \geq 6$  to identify progenitors of present-day old, low-mass stellar systems with a particular focus on GCs and forming dwarf galaxies. The aim of this is primarily to identify and classify infant GC like objects in a self-consistent way which does rely on physical properties at high redshift. We will show that two distinct groups of objects emerge. One of which are highly likely to be forming globulars and the other proto-ultra faint dwarfs. The paper is laid out as follows. In the next section, we discuss the simulations used and the two groups of objects that emerge. In Section 3, we present our initial results. We compare the properties of the infant GCs candidates in our simulations to high-redshift observations in Section 4. In Section 5, we describe the environments which we find said candidates in. Finally, we summarise our findings in Section 6. Throughout this work we assume  $H_0 = 71 \text{ kms}^{-1}\text{Mpc}^{-1}$ ,  $\Omega_M = 0.265$ ,  $\Omega_\Lambda = 0.735$   $\Omega_b = 0.0448$ .

## 2 SIMULATIONS

The numerical framework within which the present study is conducted is a simulation from the First Billion Years (FiBY) project. These are a suite of high-resolution cosmological hydrodynamics simulations. They have been performed by using a modified version of GADGET3 (Springel 2005; Schaye et al. 2010) which includes specific physics relevant for the onset of galaxy formation in the high-redshift Universe (Johnson et al. 2013). These simulations run until  $z = 6$ . All substructures within the simulations are identified with the SUBFIND algorithm (Springel et al. 2001; Dolag et al. 2009; Neistein et al. 2011).

In this work, a simulated box of volume  $(4 \text{ Mpc})^3$  with  $2 \times 684^3$  particles is used. The mass resolution of particles is  $1250 M_\odot$  and  $6160 M_\odot$  for SPH and DM particles, respectively. The co-moving Plummer-equivalent gravitational softening length is  $\epsilon = 234 \text{ pc}$  or  $\leq 33 \text{ pc}$  in physical units at  $z \leq 6$ . In the following we give a brief summary of the implemented physics and refer the reader to e.g. Johnson et al. (2013); Paardekooper et al. (2015) and Cullen et al. (2017) for more details. In the simulation, star formation occurs at a threshold density of  $n = 10 \text{ cm}^{-3}$  and has a prescription based on a pressure law designed to be consistent with the observed Schmidt-Kennicutt Law (Schmidt 1959; Kennicutt 1998; Schaye & Dalla Vecchia 2008). The simulation forms both Population II and III stars. For each of the populations a different IMF is assumed. For Population III stars, a

power-law with a Salpeter slope (Salpeter 1955) is assumed for a mass range of  $21M_\odot - 500M_\odot$ . The adopted stellar IMF for Population II stars is that of Chabrier (2003). There is a ‘critical metallicity’ at which the stellar IMF transitions between that for Population III and II stars (Maio et al. 2011). The value of this metallicity in FiBY is  $Z_{\text{crit}} = 10^{-4} Z_\odot$ . This value is consistent with prevailing theory and inferred metallicities of the most metal-poor stars (Frebel et al. 2007; Caffau et al. 2011). Stellar feedback is modelled via an injection of thermal energy from star particles to neighbouring particles (Dalla Vecchia & Schaye 2012). Once a star particle (for a Population II star) has reached an age of 30 Myr, a supernova is injected with an energy of  $10^{51}$  erg. This age is chosen as it corresponds to the maximum lifetime of stars that end their lives as core-collapse supernova. A similar technique is applied to model feedback from Population III stars, however a differentiation is made between Type II SNe (Population II stars, occurs for initial stellar masses  $8 \lesssim M_* \lesssim 100$ ) and PISNe (Population III stars, occurs for initial stellar masses  $140 \lesssim M_* \lesssim 260$ ). For the latter, an energy of  $3 \times 10^{52}$  erg per SN is injected. For metal pollution, FiBY tracks 11 elements: H, He, C, N, O, Ne, Mg, Si, S, Ca and Fe. Cooling of the gas is based on line-cooling in photoionization equilibrium for these elements (Wiersma et al. 2009) using tables from the CLOUDY v07.02 code (Ferland et al. 1998). Also incorporated into the simulations are full non-equilibrium primordial chemistry networks (Abel et al. 1997; Galli & Palla 1998; Yoshida et al. 2006), including molecular cooling for  $\text{H}_2$  and HD.

## 3 RESULTS

### 3.1 Classifying Low-Mass Systems

To identify infant GC candidates and other progenitors of small mass present-day objects within the simulations, we extract all SUBFIND identified substructures in the simulated box within the stellar mass range  $10^4 - 10^8 M_\odot$ . For each of the substructures, their total baryon fraction:

$$f_b = \frac{(M_* + M_{\text{gas}})}{M_{\text{total}}} \quad (1)$$

is calculated where  $M_{\text{total}}$  is the sum of baryonic and dark matter masses,  $M_*$  the stellar mass and  $M_{\text{gas}}$  the mass in gas. Equation 1 gives the fraction of mass contained in baryonic material. Also calculated for each of the objects is the stellar fraction. This quantity defines the amount of baryonic mass found in stars:

$$f_* = \frac{M_*}{(M_* + M_{\text{gas}})} \quad (2)$$

All the objects that were extracted from the simulations are plotted within the plane drawn out by  $f_b$  and  $f_*$ . This plane can be seen in each of the panels of Figure 1<sup>1</sup>.

In Figure 1, we discriminate between different masses of individual objects through the size of the data point. Each

<sup>1</sup> We wish to note that the sharp edge at large dark matter fractions is a result of the imposed mass limits on the stellar mass of the objects and follows the expected  $f_* \propto 1/f_b$  behaviour.

panel has a different colour-bar to add further information about the objects. In the top panel the colours indicate the stellar metallicity of the substructure. In the middle and bottom panels the colour-bar represents the total stellar and dark matter (DM) mass of the parent FOF halo that the object belongs to. We can see from Figure 1 that two distinct groups of objects emerge with respect to the general population.

The first of these groups can be seen as a vertical line where  $f_b = 1$  i.e. the total mass of these objects is in the form of baryons. Hence from their very definition, these objects have low DM fractions. They all seem to have masses in the range of  $10^4 - 10^6 M_\odot$ . From the top panel, it can be seen that a majority of these objects have a stellar metallicity which is about half solar. These objects appear to be lying within an environment that contains either a much larger host galaxy, or many other objects of a similar mass (see middle panel of Figure 1). The total stellar mass within the parent halo for all these objects exceeds  $10^6 M_\odot$ . Whilst these individual substructures appear to have a low concentration of DM within them, they lie within an extended DM halo environment (see bottom panel of Figure 1).

The second distinct group of objects lie horizontally in the plane along the  $f_* = 1$  line. These objects are similar in mass to those along the  $f_b = 1$  strip, yet they are vastly different from each other. For this second group of objects, all their baryonic matter is tied up in stars. However, their baryon fraction itself is low, indicating a large concentration of DM within these objects. When looking at their stellar metallicities, they are more metal poor than the  $f_b = 1$  objects. They have a stellar metallicity about a quarter of the solar metallicity. When comparing these  $f_* = 1$  substructures to the stellar masses of their parent haloes, it can be seen that these objects are likely to be isolated and the host galaxy themselves, as for most of the substructures the stellar mass within their parent halo is equal to the objects stellar mass. The  $f_* = 1$  group also lies within an extended DM halo, but this halo is on average two orders of magnitude smaller than the halo of the  $f_b = 1$  group.

An interesting feature of the  $f_b = 1$  and  $f_* = 1$  groups is that they are separated from the main distribution of substructures by a distinct gap, which is more apparent for the  $f_b = 1$  group of objects. Shown in the bottom panel of Figure 1 is a histogram of the distribution of objects with certain values of  $f_b$ . There is a clear valley between the universal baryon fraction and the  $f_b = 1$  objects, indicating that these objects likely are characterized by different amount of DM at birth. The non-continuous nature of the distribution argues for a distinct formation processes of  $f_b = 1$  objects.

We hypothesize that the objects along the  $f_b = 1$  line can be associated with infant GC systems, whilst the  $f_* = 1$  objects could be akin to proto-ultra-faint dwarfs (UFDs) as we will discuss in the following. In order to test these hypotheses, we compare the  $f_b = 1$  and  $f_* = 1$  groups and three sub-samples of objects which have been chosen based on observational constraints in the local Universe. The first of these sub-samples is stellar mass limited within the range  $10^4 \leq M_\odot \leq 10^7$ . Whilst not all the objects in this mass range will be either an infant GC or a UFD, being able to compare the properties of these two distinct groups of objects to a more general population will help discriminate how unique they are. The second sub-sample contains objects within the

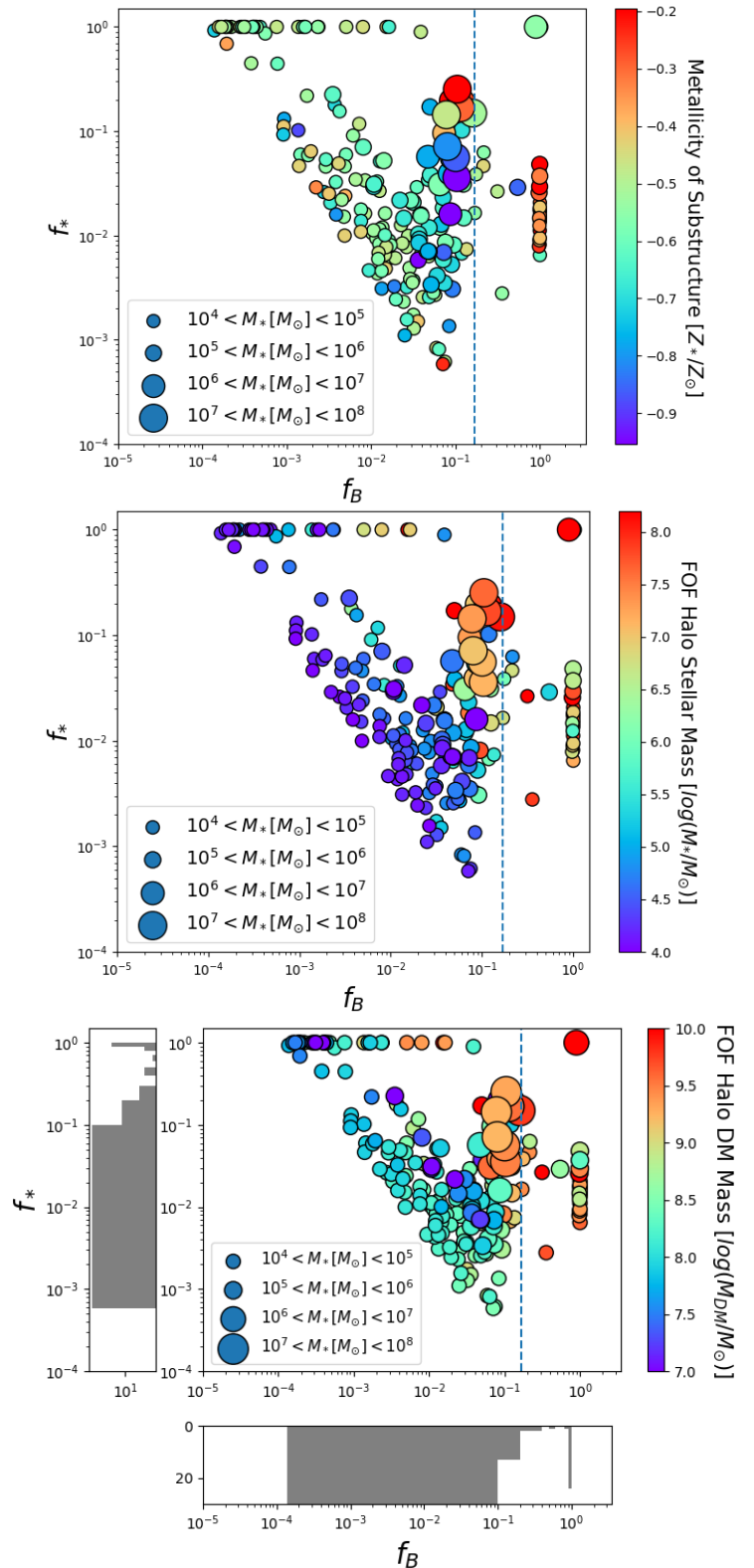


**Figure 1.** Fraction of baryons in stars ( $f_*$ ) plotted against the total fraction of baryons ( $f_b$ ) for all substructures identified by *SUBFIND* in the stellar mass range of  $10^4 \leq M_* [M_\odot] \leq 10^8$  at  $z = 6$ . The sizes of the symbols indicate the mass range of the substructures. The vertical line represents the *WMAP* 7-year universal baryon fraction value of 0.167 (Komatsu et al. 2011). From top to bottom the colour bars represent; the stellar metallicity of the substructures, the stellar mass of the parent Friend-of-Friend (FOF) halo, and the dark matter mass of the parent FOF haloes.

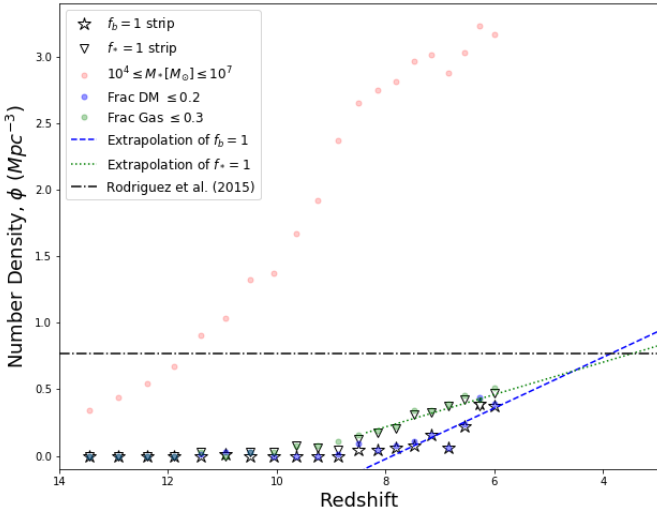


**Figure 2.** Redshift evolution of the number density of potential candidate GCs in the simulation. Stars and triangles represent the  $f_b = 1$  and  $f_* = 1$  groups. Pale coloured dots indicate the observationally constrained subsamples we are comparing to. The solid and dot-dash lines are predicted values of  $\phi$  taken from the literature (see legend and Section 3.2).

same mass range as before, but that also have a dark matter fraction  $\leq 0.2$ . Such a condition was chosen in order to allow a broader assessment of stellar systems in the regime of relatively low DM fraction, without imposing a strict requirement of a complete absence of DM (see Section 1 for some phenomenological considerations on this specific issue). Therefore, whilst it is likely that GCs formed within an extended dark matter halo, here we focus on the analysis of objects with a relatively low intrinsic DM content. The final sub-sample has a gas fraction of  $\leq 0.2$  and stellar masses in the range  $10^4 \leq M_\odot \leq 10^7$ . This constraint comes from the current understanding of UFDs. These particular dwarfs appear to have a very low gas content (Brown et al. 2014; Westmeier et al. 2015; Simon 2019). Thus it would be interesting to see how the properties of the  $f_* = 1$  group compare to this sub-sample.

In the rest of this paper the main focus will be the  $f_b = 1$  objects, but will also analyse some of the properties of the  $f_* = 1$  objects.

### 3.2 Number Density of the GC Candidates

As a first step, we are comparing below the number density of present-day GCs with those of the different populations that we have identified at  $z = 6$ . We will focus as well on the build-up of the  $z = 6$  population of infant GCs.

In Figure 2, we plot the evolution of the number density ( $\phi$ ) as a function of redshift for both the  $f_b = 1$  and the  $f_* = 1$  objects. The number density is calculated by dividing the total number of objects on each strip by the volume of the simulated box (see Section 2). A recent estimate of the local number density of GCs is illustrated with an horizontal dot-dashed line (at  $0.77 \text{ Mpc}^{-3}$ ; for further details of such a calculation see Appendix 1 in Rodriguez et al. 2015).

By comparing our findings to the local Universe litera-

ture, we see that our infant GC candidates are characterized by a lower value for  $\phi$ . However, GCs are expected to still be able to form until  $z \sim 3$  (Katz & Ricotti 2013; Kruijssen 2015). The value of  $\phi$  we estimate in our simulations for infant GCs is about half of that quoted by Rodriguez et al. (2015), suggesting that a significant fraction of GCs will still form after  $z = 6$ . Through an extrapolation of the number density to  $z = 3$  as based on the trend we see in number densities for both  $f_b = 1$  ( $d\phi/dz = -0.19$ ) and  $f_* = 1$  ( $d\phi/dz = -0.12$ ) objects between  $z = 8$  and 6, we easily match the local observed number densities of GCs. However, we wish to stress that such an extrapolation does not take into account any disruption of GCs. On the basis of this approximated approach, only  $\sim 80\%$  of the population at  $z = 3$  would need to survive to ensure agreement with local observations.

An interesting result that arises from Figure 2 is that the number density for the  $f_b = 1$  and  $f_* = 1$  objects match the one for the DM (blue dots) and gas (green dots) constrained subsamples based on local-Universe observations of GCs and UFDs. This is not surprising when recalling the results from the bottom panel of Figure 1. As noted, there is a distinct gap between the  $f_b = 1$  and  $f_* = 1$  objects and the other substructures we have identified. Therefore, any cut in baryon fraction above 0.167 would result in a subset of objects which would contain our infant GCs. In a follow-up study we will focus on the origin of this gap in the context of the formation and evolution of these objects.

### 3.3 Global Properties of the GC Candidates

We proceed by studying the global properties of our GC objects. These properties will allow us to further analyse the difference between the  $f_* = 1$  and  $f_b = 1$  group of objects, and to validate the hypothesis that the  $f_b = 1$  objects are indeed infant-globulars. In addition, such a global characterisation may provide initial constraints and predictions for future high-redshift observations of GCs. We wish to focus on the following global properties; stellar half-mass radius ( $R_*$ ), stellar density ( $\rho_*$ ), stellar metallicity ( $Z_*$ ) and stellar velocity dispersion ( $\sigma_*$ ). These were chosen as they are both directly accessible via observations and simulations.

We established two distinct groups of objects covering a similar mass range in the  $f_b - f_*$  plane in Figure 1. In Figure 3, we investigate whether a clear separation exist for global properties when split up by stellar mass ( $M_*$ ).

The general picture emerging from Figure 3 is that the two distinct groups of objects found in Section 3.1 (denoted by stars and triangle symbols, respectively) continue to be well separated in terms of their sizes, metallicity and velocity dispersion. However, within each group, a dependence on the stellar mass of all examined global properties can be noted. As discussed in the previous Section, it appears that the  $f_b = 1$  objects and the DM fraction-limited sample consist of the same objects, as they overlap within the same regions of the parameter spaces illustrated in Figure 3. The same can be said for the objects in the  $f_* = 1$  group and gas fraction-limited sample. We interpret this equivalence mainly as a consequence from the gap that appears in Figure 1 (see Section 3.1 for more details).

The top left panel in Figure 3 shows our reference mass-size plane ( $R_*$  vs  $M_*$ ). For the simulation data,  $R_*$  is calcu-

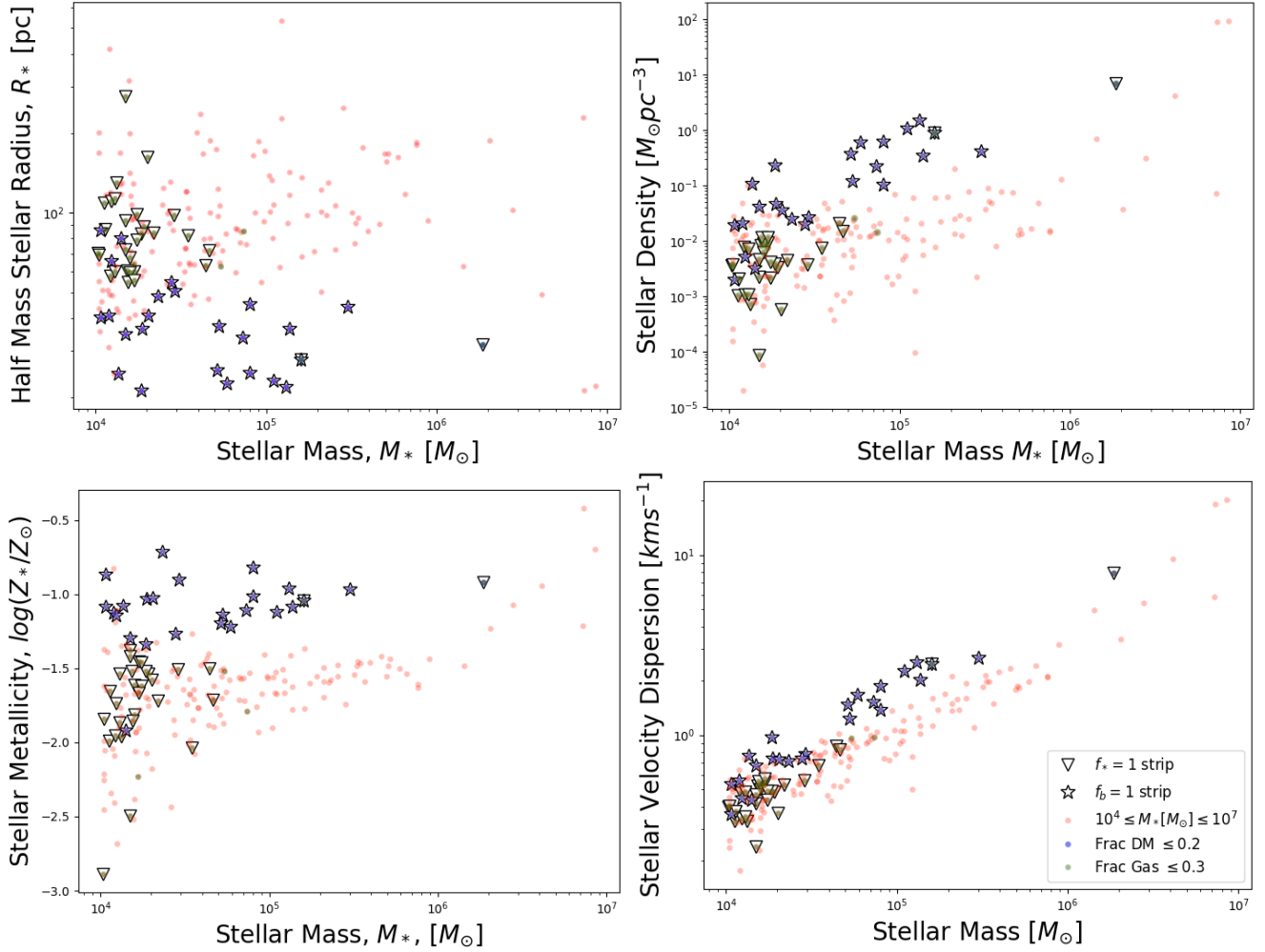


**Figure 3.** From top left to bottom right: stellar radius, stellar density, stellar metallicity and stellar velocity dispersion as a function of stellar mass. Pale dots indicate the sub-samples defined using observable properties of present day GCs (see Section 3.1). Stars and triangles represent the  $f_b = 1$  and  $f_* = 1$  samples, respectively. Stellar density is calculated assuming spherical symmetry, whilst the stellar velocity dispersion is calculated using the virial theorem (see Section 3.3).

lated by using particle information as follows. For each of the objects, the coordinates of the most bound particle are obtained (star, gas or dark matter particle). This most bound particle represents the minimum of the potential well for a given object and we identify this as its centre. By assuming spherical symmetry, the number of star-particles within a spherical shell of a given size is counted. The radius of the shell is increased from zero in increments of 0.1 pc. The value of  $R_*$  is then obtained by plotting a cumulative stellar mass profile for the object as a function of radius and then choosing the radius which encloses 50% of the stellar mass. From such mass-size plane, it can be seen that the objects we call infant GCs candidates ( $f_b = 1$  objects) are the most concentrated and have the smallest radii out of all identified objects in the simulation. They all have radii  $< 90$  pc, with a majority of our infant GCs having radii in the range  $40 - 60$  pc<sup>2</sup>. The systematically lower value of  $R_*$  for these objects holds across a broad range of stellar masses,

indicating that this is a general property for objects of this classification. Confirmation that these objects are compact is further evidence to support the notion that the  $f_b = 1$  objects are plausible infant GC candidates. The  $f_* = 1$  group appears to span a broad range of stellar radii ( $\sim 60 - 300$  pc, with two objects  $< 60$ pc) for a given stellar mass, showing that these objects are more diverse, but crucially different to the sizes of the objects in the  $f_b = 1$  and DM fraction-limited samples. By comparing the objects from the  $f_b = 1$  and  $f_* = 1$  groups, we can see that the majority of the latter are  $\sim 1.5 - 7\times$  larger than the former. In the local Universe, GCs are typically observed to have half-light radii of the order of  $\sim 10$  pc (Harris 1996; Larsen et al. 2002; Masters et al. 2010, e.g., see) and for UFDs  $\sim 30 - 100$  pc (e.g., see Bechtol et al. 2015; Koposov et al. 2015; Simon et al. 2015). Thus the ratio of sizes we find between our infant GCs and UFDs are similar to the ratio of sizes of these objects at  $z = 0$ .

In the second panel of Figure 3 the stellar density,  $\rho_*$

<sup>2</sup> The gravitational softening (33 pc at  $z = 6$ ) is of similar order as the size of these objects. We therefore expect the sizes to be

overestimated, especially for the most compact objects. General relative trends between populations however, should be robust.



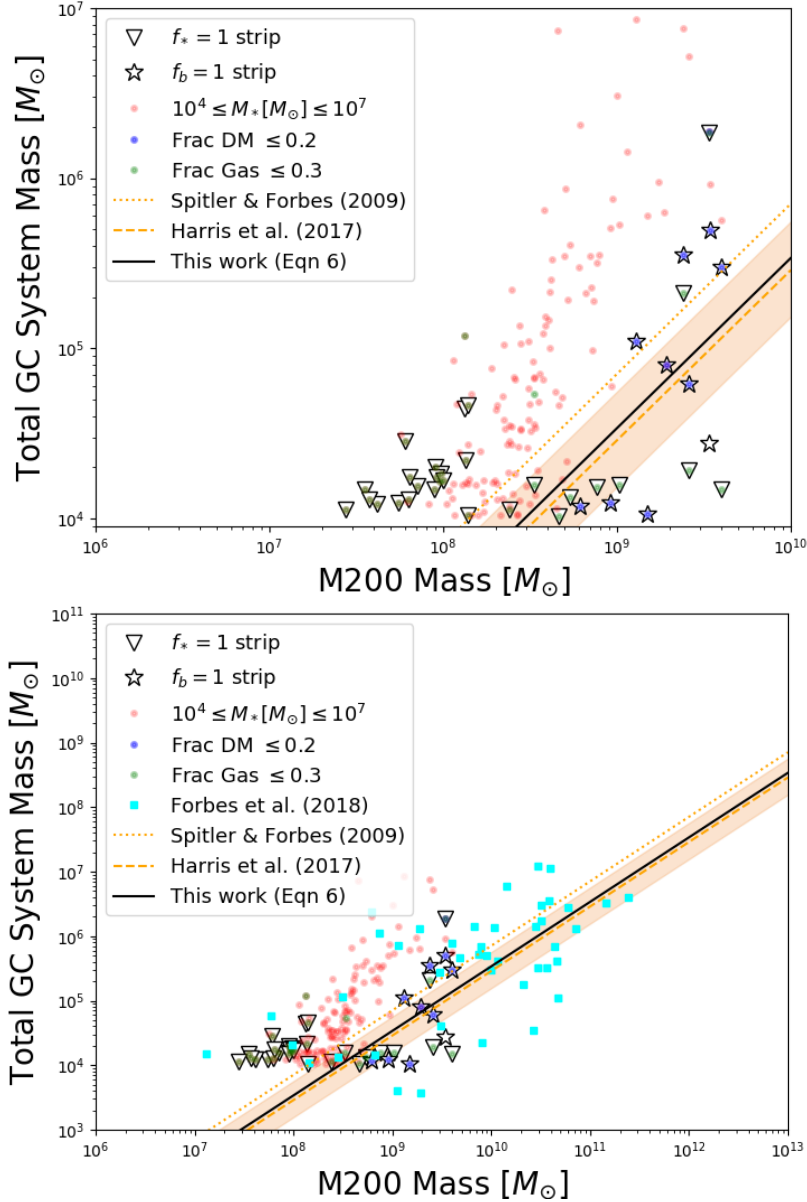


**Figure 4.** Top: The total stellar mass of potential GC systems plotted against their parent halo mass. Pale dots indicate sub-samples defined using observable properties of present day GCs. Stars and triangles represent the  $f_b = 1$  and  $f_* = 1$  samples, respectively. Two of the relations plotted are taken from Spitler & Forbes 2009 (solid) and Harris et al. 2017 (dash). The yellow line is the relation we find for our simulated data. Bottom: same as top plot except the turquoise squares are the GC systems examined in Forbes et al. (2018b)

is plotted. With reference to the approach described above to calculate the stellar half-mass radius, we estimate  $\rho_*$  by using the mass within  $R_*$ . Consistently with their behaviour in the mass-size plane, the objects in  $f_b = 1$  group appear to be the densest identified in our simulation. There is also a trend that the more massive objects in this group are more dense by about one order of magnitude compared to other objects of the same mass, again fitting with the behaviour observed for stellar radii. These relatively high stellar densities (compared to the other sub-samples) calculated for the  $f_b = 1$  objects further reinforce the intuition of them being infant GCs. Local measurements of GC densities (e.g., see McLaughlin & van der Marel 2005) are typically larger than those in our simulation. This is a consequence of the force

resolution in our simulation which results in the radii being over-estimated.

The bottom left panel of Figure 3 shows stellar metallicity,  $Z_*$  against stellar mass. Amongst the simulated objects, there appears to be a clear distinction between the  $f_b = 1$  group and the  $f_* = 1$  group. The infant GC objects (star symbols) appear to be a factor two more metal-rich than the general population and show a spread of  $\sim 1$  dex. The range of metallicities we are finding for our infant GCs is consistent with local observations of GC metallicities. Although in the local Universe, there are some Galactic GCs which have a higher metallicity than what we find by  $\sim 0.5$  dex (e.g., see Brodie & Huchra 1991; McLaughlin & van der Marel 2005; Muratov & Gnedin 2010).

The final panel in Figure 3 shows the stellar velocity dispersion - mass plane ( $\sigma_*$  vs.  $M_*$ ). A simple estimate based on the virial theorem:

$$\sigma_* = \sqrt{\frac{1}{2} \frac{G M}{R_{\text{half}}}} \quad (3)$$

was used to calculate the value of the velocity dispersion. There is an obvious positive correlation between  $\sigma_*$  and  $M_*$ , which results mainly from the virial theorem itself. As expected, for denser systems, i.e.  $f_b = 1$  objects, the velocity dispersion is higher.

### 3.4 GC System Mass - Halo Mass Relation

An observational scaling law of GCs that has been looked at in depth is that between the total mass of GCs associated with a host galaxy ( $M_{\text{GC}}$ ) and the mass of the host halo ( $M_{\text{Halo}}$ ). This is a linear relation (e.g., see Spitler & Forbes 2009; Hudson et al. 2014; Kruijssen 2015; Harris et al. 2015, 2017), showing that more massive galaxies have a greater GC system mass. So far, only low-redshift observations of such a scaling relation exist. Knowledge of the shape of this relation around the epoch when the GCs formed the majority of their stars ( $z \geq 6$ ) will put constraints on the subsequent evolution of GC systems and the connection to their host galaxies. Also, if this relation is already established at high redshift, then this could hint at a conformity across all different masses of GC systems in terms of their future evolution.

In Figure 4, we have depicted the estimated GC system (stellar) mass against the FOF halo mass from the simulation ( $M_{200}$ ). On this plot, illustrated as the dashed lines are the system mass – halo mass relations from Spitler & Forbes (2009), SF09, and Harris et al. (2017), H17. The relation found in SF09 is a simple linear relation between the two quantities:

$$\log\left(\frac{M_{\text{GC}}}{M_{\text{Halo}}}\right) = -4.15 \quad (4)$$

In their work,  $M_{\text{GC}}$  is calculated by multiplying the number of GCs per galaxy by an average GC mass of  $4 \times 10^5 M_{\odot}$ .  $M_{\text{Halo}}$  is defined as the total mass (baryonic plus dark matter) within a sphere containing an over-density of 180 times the background.<sup>3</sup>

The relation found in H17 is close in appearance to that of SF09:

$$\log\left(\frac{M_{\text{GC}}}{M_{\text{Halo}}}\right) = -4.54 \quad (5)$$

where the values  $M_{\text{GC}}$  and  $M_{\text{Halo}}$  are calculated in a similar way as in SF09. In H17, however, they assume a mean GC mass which varies with galaxy luminosity. There is a residual RMS scatter in the H17 relation of  $\pm 0.28$  dex (shown as the grey shaded region in Figure 4).

For the  $f_b = 1$  sample (the most likely GC candidates)

<sup>3</sup> This is slightly different to the halo mass we use, which is the  $M_{200}$  mass, i.e. a sphere containing an over-density 200 times the background. We looked into the difference when using  $M_{180}$  and found very little change. We therefore decided to present the relation for  $M_{200}$  which is commonly used in numerical studies.

each of the relations could be regarded as a reasonable fit, although the limited range in mass of  $M_{\text{GC}}$  probed in our sample restricts how well this can be quantified, particularly at masses  $M_{\text{GC}} \geq 10^6 M_{\odot}$ . The latter is mainly due to the limited simulation volume. We find evidence suggesting that  $M_{\text{GC}} - M_{\text{Halo}}$  relation exists at  $z = 6$  in our simulation. Such a relation is similar (with a normalization for a fixed slope) to the one observed at  $z = 0$ , with

$$\log\left(\frac{M_{\text{GC}}}{M_{\text{Halo}}}\right) = -(4.47 \pm 0.15) \quad (6)$$

although a larger mass range would help support these claims. However, the individual observations presented by Forbes et al. (2018b) agree well with the simulated data in terms of actual values and scatter. Interestingly, for the rest of the simulated population however, the observed relations appear to underestimate the system mass, further supporting that the selection of objects adopted in this analysis, as based on their dark matter fraction identifies likely GC candidates.

The comparison to the local relation puts bounds on the future evolution of the different groups identified in this analysis, especially regarding the mass evolution of individual objects, as resulting from internal and external processes. The  $f_b = 1$  population of objects leave little room for such processes to take place if they are to match the local relation without the formation of new GCs at  $z < 6$  or residual star formation from existing gas in infant GCs. In contrast, the general population of objects in the corresponding mass range would need to loose up to one order of magnitude in mass and/or grow significantly slower in mass than their hosting halo to be consistent with the local relation. From the bottom panel of Figure 4 there is a good indication that a relation between  $M_{\text{GC}}$  and  $M_{\text{Halo}}$  is already in place by  $z = 6$ .

As both the SF09 and H17 relations are linear, the expectation is that, as the haloes of infant GC systems merge with other halos, the resultant relation will continue to follow the local one. The  $M_{\text{GC}} - M_{\text{Halo}}$  scaling relation observed in the local Universe would result from the variation in the growth history of the GC systems and any processes related to stripping of stars and ongoing star formation. The scatter we find in the relation at  $z = 6$  is 0.46 dex. This is larger than the 0.28 dex scatter H17 found for the  $z = 0$  relation. However, continued merger during the hierarchical growth of the host results will result in a decrease of the scatter due to the central limit theorem (Hirschmann et al. 2010; Jahnke & Macciò 2011).

## 4 COMPARISON WITH HIGH REDSHIFT OBSERVATIONS

Observations in the early Universe of infant GCs are currently limited by the intrinsic difficulties posed by the detection and characterization of low-mass stellar systems at high redshifts. Even in the local Universe, it is hard to accurately measure the mass and luminosity of GCs surrounding their parent galaxies. This task becomes more even laborious when moving to higher redshift. However, with JWST on the horizon, the potential for studying these systems at formation looks promising (see Section 1 and especially the



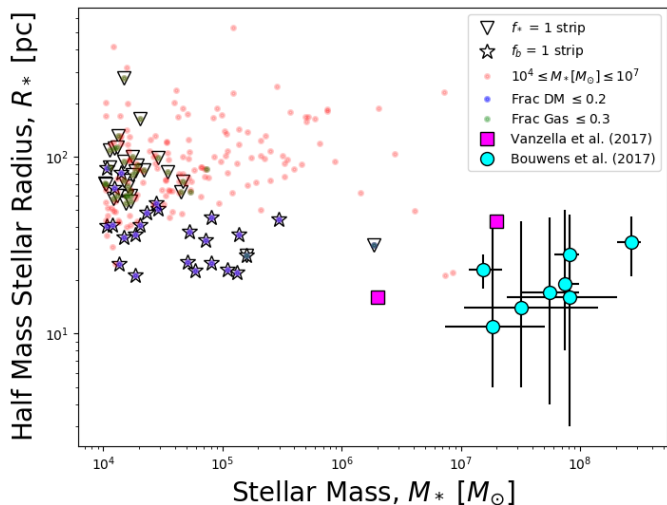


**Figure 5.** Stellar radius versus stellar mass. Pale dots indicate sub-samples defined using observable properties from the local Universe. Stars represent our infant GC candidates and triangles our proto-UFDs. The magenta circles and cyan squares are high redshift observations from Vanzella et al. (2017) and Bouwens et al. (2017) respectively. For the Bouwens et al. (2017) data, we have taken objects from their Table 2 which had a radius  $< 50$  pc including errors.

recent studies by Renzini 2017; Forbes et al. 2018a; Pozzetti et al. 2019).

There has been some preliminary work in observing candidate GCs at  $z > 3$ . For example, Vanzella et al. (2017) identified a selection of objects at redshifts,  $z = 3.1169, 3.235$  and  $6.145$ . A few of these objects are very promising potential infant GCs (see magenta squares in Figure 5). Table 1 in Vanzella et al. (2017) summarizes the physical properties and magnifications for the most magnified images in the systems they studied. In particular, GC1 and ID11 are the most likely infant GC candidates in their sample. They have half-light radii consistent with what we are finding in our simulation (i.e.  $\leq 50$  pc). However, the measured masses of GC1 and ID11 are more than an order of magnitude larger than the masses of the  $f_b = 1$  strip objects being identified in the present study. This is mainly due to the limited volume of the simulations, and the choice of an average density in the volume, which does not allow to probe massive systems.

Three of the five objects studied by Vanzella et al. (2017) are also included in the sample of objects investigated by Bouwens et al. (2017). In their study, a sample of 307 faint sources from the Hubble Frontier Fields (HFF) is examined, with all sources located at  $z = 6 - 8$ . A selection of such objects (see their Table 2) have half-light radii  $\leq 40$  pc. It is likely that some of these objects could be infant GCs, especially when compared to observational data from the local Universe (their Figure 10). Whilst some of these objects are more extended than a typical GC, these sizes are consistent with what we are finding in the FiBY simulations. Taking these results at face value we would expect very little size evolution across four orders of magnitude for GCs in the high-redshift Universe.

Due to their relatively short relaxation times, as well as tidal interactions with their host galaxies, GCs evolve signif-

icantly in mass and size, as due to the cooperation of internal and external processes, giving origin to the structural and kinematic properties we measure at  $z = 0$ . Therefore, the consistency we are finding with preliminary observations of high redshift GCs and our candidates in the FiBY simulations indicates that the results in Figure 3 are encouraging and can serve as an upper limit when making predictions for future observations.

## 5 INFANT GC ENVIRONMENTS

Finally, we move on to the analysis of the environments for our most likely infant GC candidates. By gaining insight into the formation environments of globulars, one can begin to establish which channel they formed through (see Section 1). In the local Universe, GCs are often found to be members of collective systems associated with a host galaxy (e.g., see Harris 1991; van den Bergh 2000; Harris et al. 2013). In Local Group galaxies, the general expectation is that GCs are composed of both in-situ and accreted star clusters, but the fraction of GCs accreted at low redshift is still under intense evaluation (e.g., see Côté et al. 1998; Tonini 2013; Renaud et al. 2017; Recio-Blanco 2018). Therefore, it is important to include in this study an environmental analysis. Indeed, we have already shown in this work that our infant GC candidates lie within extended dark matter haloes (see Figure 1, Section 3.1). Many of them also already seem to be part of a larger GC system which follows the known GC system mass – halo mass relation (Figure 4, Section 3.4). In this Section, we look deeper at the current ( $z = 6$ ) environments of our infant GCs.

For each of the candidates identified in Section 3.1, their parent FOF halo was located. The 24 candidates are distributed across 10 different FOF halos. The largest system contains 6 infant GCs whilst some halos only contain 1 candidate. Within each FOF halo, the largest SUBFIND member was identified. This member is labelled as the host galaxy of the GC system.

In Figure 6, we show the positions of the infant GC candidates (star symbols) in the x-y plane of the simulation. The positions of our candidates are illustrated in a frame of reference centered on the center of mass of the host FOF halo as well as the (likely) parent galaxy (orange and purple crosses, respectively). The  $R_{200}$  of the FOF halo and half mass radius  $R_{half}$  of the host galaxy are plotted as circles of orange and purple colour, respectively. Finally, the colour map represents the underlying distribution of DM particles belonging to the FOF halo. Darker colours indicate regions with a higher density of DM particles i.e. a density peak.

When considering the DM density distribution in Figure 6, one can see that the infant GC objects are preferentially found at the density peaks for their given FOF. This is consistent with the expectation that structures form in density fluctuations (Blumenthal et al. 1984; Kaiser 1984; Peebles 1984; Davis et al. 1985; Springel et al. 2005), however we note that our infant GC candidates contain a low number of DM particles which are energetically bound to the system. Keeping in mind the limitations determined by the numerical resolution and volume of our cosmological simulation (see Section 2), we compare the number of DM particles bound to our infant GCs and the number of DM particles that lie

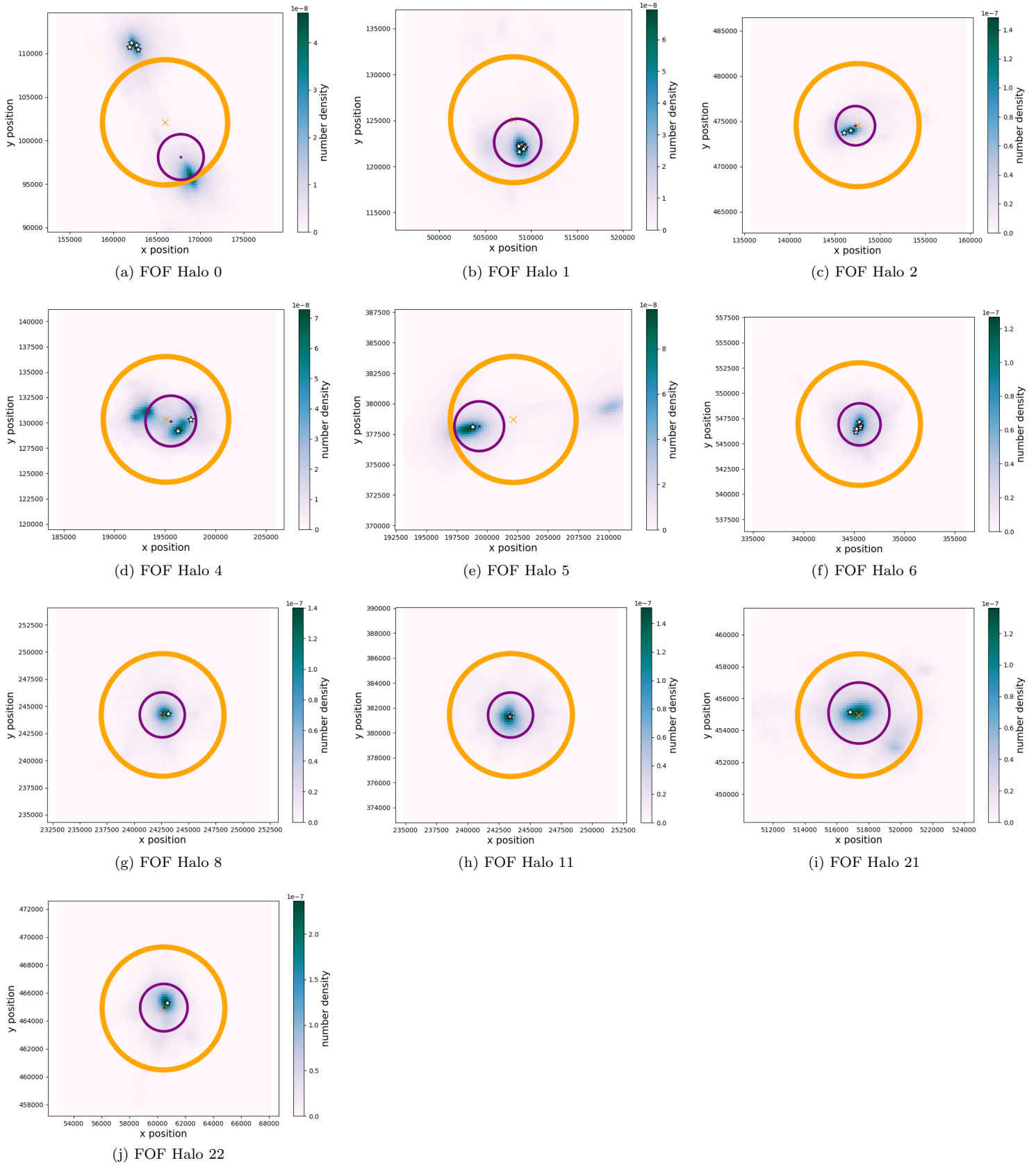


**Figure 6.** Postions of our most likely infant GC candidates within their respective parent FOF halo. The star symbols represent the infant GCs indentified in Section 3.1. The orange and purple circles represent the positions and radii of the FOF halo and the associated parent galaxy, respectively (see text for further details). The colour map traces the underlying density distribution of the DM particles belonging to the FOF halo.

FOF ID	FOF $R_{200}$ (kpc)	Gal ID	Gal $R_{half}$ (kpc)	Gal $M_*$ ( $M_\odot$ )	Num of GCs	$M_{cl}$ ( $M_\odot$ )	$d_{gal}$ (kpc)	$v$ (km/s)
0	7.20	0	2.62	$9.40 \times 10^7$	4	$5.4 \times 10^6$	14.58	21.3
						$4.09 \times 10^6$	13.53	18.4
						$3.57 \times 10^6$	14.27	26.5
						$1.29 \times 10^6$	14.03	14.8
1	6.84	68	2.57	$6.14 \times 10^7$	6	$1.02 \times 10^7$	0.6202	20.2
						$3.10 \times 10^6$	0.45587	20.1
						$2.08 \times 10^6$	1.05	23.0
						$2.01 \times 10^6$	0.94701	19.4
						$1.38 \times 10^6$	0.41287	24.2
						$9.82 \times 10^5$	0.96094	17.3
2	6.81	141	2.18	$1.21 \times 10^7$	2	$2.17 \times 10^6$	1.62	24.6
						$9.22 \times 10^5$	0.79688	17.6
4	6.21	261	2.50	$4.10 \times 10^6$	2	$1.50 \times 10^6$	1.26	5.75
						$1.39 \times 10^6$	2.10	7.77
5	5.17	286	2.04	$4.27 \times 10^7$	1	$6.78 \times 10^5$	0.55959	16.1
6	6.07	316	2.08	$7.25 \times 10^6$	5	$3.12 \times 10^6$	0.81133	9.63
						$2.75 \times 10^6$	0.27059	8.87
						$1.57 \times 10^6$	0.55919	11.9
						$9.95 \times 10^5$	0.37954	21.7
						$1.59 \times 10^5$	0.29052	10.9
8	5.65	392	2.07	$2.11 \times 10^7$	1	$2.35 \times 10^6$	0.59289	12.0
11	4.94	472	1.81	$8.51 \times 10^6$	1	$3.01 \times 10^6$	0.16266	7.00
21	3.84	714	1.91	$2.03 \times 10^6$	1	$8.28 \times 10^5$	0.86058	4.73
22	4.40	737	1.70	$4.97 \times 10^5$	1	$1.00 \times 10^6$	0.42662	4.63

\*Note: in this Table we list the galaxy's stellar mass but for the infant GCs we list their total mass (stellar plus gas).

**Table 1.** Table giving the identifiers for each of the FOF halo, parent galaxy and infant GC as identified in the simulation. For each FOF halo, its  $R_{200}$  radius is given. For each of the (assumed) parent galaxies, the galaxy's half mass radius ( $R_{half}$ ), stellar mass ( $M_*$ ) and number of infant GCs belonging to the system is given. We provide for the infant GCs, their total cluster mass ( $M_{cl}$ ), distance from the parent galaxy center ( $d_{gal}$ ) and their orbital velocity ( $v$ ).

within the half-mass radius of the candidates. Whilst there are only relatively few stellar particles bound to each of these infant GCs, there is also a low number ( $< 40$ ) of DM particles in the underlying medium. For the most extreme case, if the underlying population of DM particles were included in the calculation of  $f_b$ , then the fraction would decrease from 1.0 to 0.8, hence this object would still be dominated by baryonic matter and classified as an infant GC. This result bares the question: how is it that our candidates can form in such a DM-rich region and yet be void of DM matter themselves? This could possibly be due to the physical mechanism underpinning the evolution of these objects. Indeed, initially the DM density peak could have resulted in a coalescence of gas at that point. As the gas cooled and contracted, star formation could begin. As the cluster then evolved, the cooperation between internal dynamical processes and external interactions with its environment (for example with its host galaxy) could result in the DM being removed from the stellar system. This is an evolutionary scenario that we will explore further in future work, where these systems will be studied at higher redshifts.

For all the GC systems - apart from the system in panel (a), a merger - the globulars lie within the half-mass radius of the host galaxy. This is indicative that tidal and dynamical interactions may have occurred during the formation of these infant GCs. We provide complimentary information to Figure 6 in the form of Table 1. As one can see from Table 1, a majority of the infant GCs (excluding those in FOF halo 0) lie  $< 1$  kpc from the center of the (assumed) par-

ent galaxy. The close proximity to the galaxy center further support the idea that these systems undergo many interactions during their first few Myr of evolution. However, the distances between our globulars and the galactic centers are much smaller than what is observed in the local Universe.

A relation is present when comparing the masses of the of the infant globulars to the stellar masses of their host galaxies. The amount of stellar mass present in a host galaxy that is required to host a most massive cluster of mass,  $M_{cl}$ , increases linearly with  $M_{cl}$  (see also Ma et al. 2019). This can be seen both in Table 1 and also in Figure 7. In this Figure, we plot the stellar mass of the parent galaxies against the number of GCs per system (top), total mass of the GC system (middle) and the total mass (stellar and gas) of most massive GC (bottom). In the middle and bottom panels we have also provided the one-to-one relations (red) and our own fits to the data (blue). In the bottom panel is displayed the linear relation between parent galaxy stellar mass and the most massive infant GC. This relation has the form:

$$\log(M_{cl}) = (0.31 \pm 0.15) \log(M_{*,gal}) + (4.17 \pm 1.06) \quad (7)$$

Finally, we discuss FOF halo 0 - panel (a) in Figure 6. This system appears to be a merger between two galaxies. To confirm this, we look at this GC system through different projections and at different times in its evolution. From this analysis, we conclude that the system is likely an ongoing merger. However, this classification results in a different problem. Is the parent galaxy identified in panel (a) of Figure 6 the original parent of the GC system? Or are the GCs

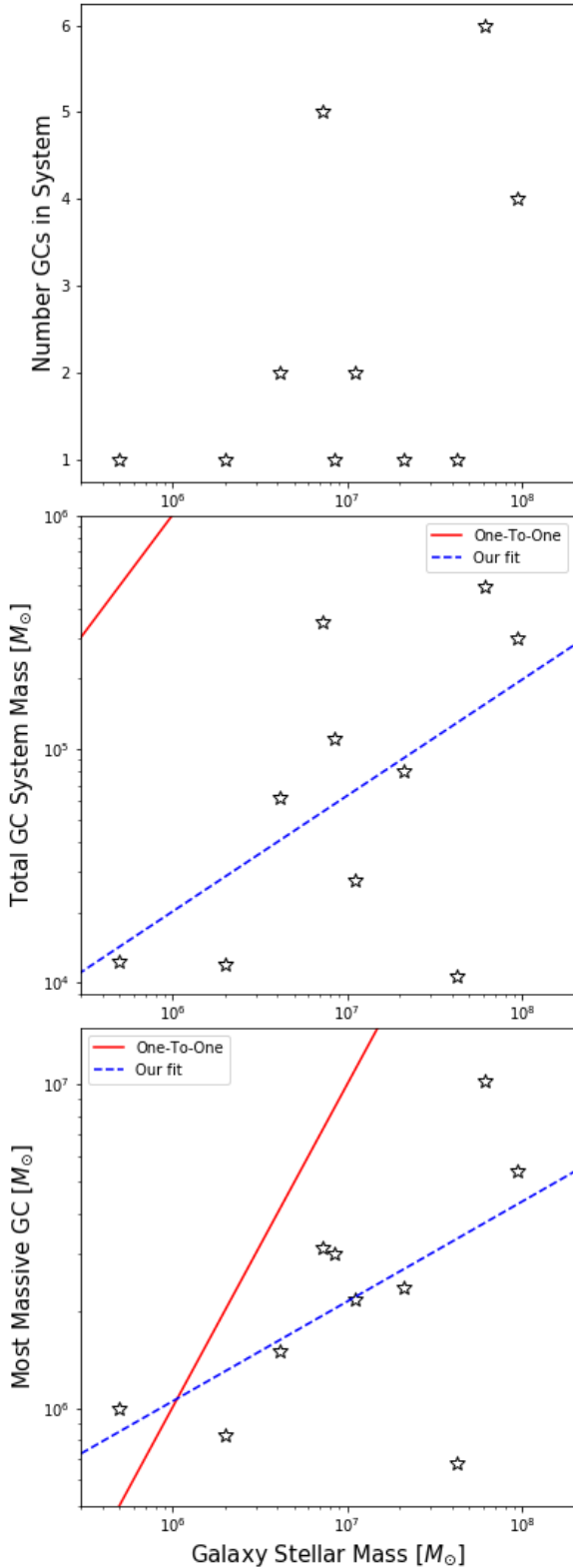


**Figure 7.** Plot of GC system number (top), GC system mass (middle) and total mass (stellar and gas) of the most massive GC (bottom) versus the stellar mass of the parent galaxy. In the middle and bottom panels, we also display the one-to-one relation (red) and our own fits to the data (blue). Further information on our fits can be found in Section 5

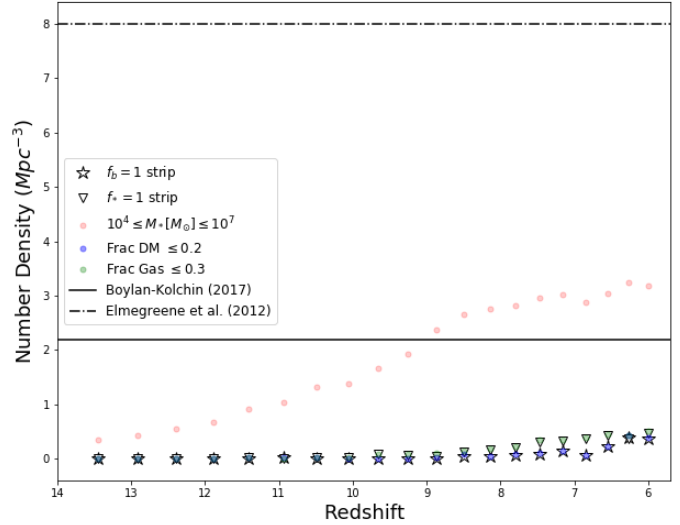


**Figure 8.** Redshift evolution of the number density of potential candidate GCs in the simulation. Stars and triangles represent the  $f_b = 1$  and  $f_* = 1$  groups. Pale coloured dots indicate the observationally constrained sub-samples we are comparing to. The solid and dot-dash lines are predicted values of  $\phi$  taken from the literature (see legend and Section 6).

in the system going to be accreted by this galaxy? From Table 1, we can see that the average distance between the infant GCs in FOF halo 0 and the parent galaxy is  $\sim 14$  kpc. Whilst this value is consistent with local Universe observations, it is much larger than the distances we are finding for the other GC infant systems further suggesting that parent shown in panel (a) of Figure 6 is not the original parent of these infant GCs. Instead, this will be the future parent of the clusters once the merger is complete.

## 6 DISCUSSION AND CONCLUSIONS

We have explored a suite of high-resolution cosmological simulations from the First Billion Years (FiBY) project at  $z \geq 6$  to identify potential globular cluster candidates during their infant stages. Two distinct groups of objects were identified within the simulations. The first of these groups of objects has a high baryon fraction and appears to lie within an extended DM environment. We associated these objects with proto-globular or infant globular clusters (GCs). The second group of objects that exhibit a high stellar fractions exhibit similarities to ultra-faint dwarf galaxies (UFDs).

We explored the likelihood that the objects with high baryon fraction ( $f_b = 1$  objects) could be infant GCs by studying their global properties as well as looking into their environments. We started by comparing the number density of infant GCs we found in the simulations with values obtained from observations at  $z = 0$ . As well as investigating consistency with low redshift observations, we will now compare what we found in Figure 2 with theoretical predictions from the literature for the number density at  $z = 6$ . This can be seen in Figure 8. The horizontal lines overlaid on Figure 8 represent two predictions for  $z = 6$  from the literature for the value of  $\phi$  as based on a combina-

tion of model assumptions on top of present-day observations of GCs; Boylan-Kolchin 2017 (solid) and Rodriguez et al. 2015 (dashed). We will briefly discuss how each author came to their predicted value, but further information can be found in their papers. Boylan-Kolchin (2017) gives a value of  $\sim 2.2 \text{ Mpc}^{-3}$  for  $N_{\text{GC}}$  at high redshift. To obtain this value, they assumed the mass function of GCs to be log-normal. Elmegreen et al. (2012) focus on metal-poor GCs and they estimate a high-redshift number density of  $8 \text{ Mpc}^{-3}$  by evolving the present-day value of  $N_{\text{GC}}$  from Portegies Zwart & McMillan (2000), with some considerations about the behaviour of metal-poor GCs. They assume that metal-poor GCs make up two thirds of the GC population and that, by  $z = 0$ , half of the GCs have evaporated. The apparent discrepancy between the model predictions and our simulations suggest that evolutionary trends in our simulations are different to the model assumptions used in both studies. In particular, assumptions based on global properties at  $z = 0$  seem not to translate directly to high-redshift behaviours. Therefore, once more observations of globulars at high redshift will progressively become available, a direct comparison between the  $N_{\text{GC}}$  assessed from such observations and the corresponding estimates based on simulations and theory should be made to constraint the physics at play. When studying the global properties of low-mass stellar systems in our cosmological simulation, we found that infant GC candidates have relatively higher stellar densities when compared to other substructures. However, the densities calculated are lower than those found in the local Universe for the Galactic GC system. This is due to a limitation of the simulations. The values of  $R_*$  determined here are likely overestimated due to the finite spatial resolution of FiBY. As well as investigating stellar density, we also looked into stellar half-mass radii, stellar velocity dispersion and stellar metallicity. When considering  $Z_*$ , we found that the infant GCs are a factor of two more metal-rich than the rest of the substructures extracted from FiBY. These values of  $Z_*$  found for our GC objects are in fair agreement with the metallicities inferred for local Galactic GCs. However, we do find that our simulations are giving slightly higher metallicities than found at low redshift. This is primarily due to enrichment process in FiBY acting too rapidly (Cullen et al. 2019).

We also investigated the GC system mass – halo mass relation: the very good agreement between the local and the  $z = 6$  relation in our simulations is somewhat surprising given that evolution of the GCs is still expected past  $z = 6$ . Most likely, the number density of infant GCs is still increasing at  $z < 6$ , which would increase the GC system mass per halo. Contributing to a further increase is the fact that many of the infant GCs have significant gas fractions that could lead to star formation at  $z < 6$ , if feedback effects are not sufficiently efficient. On the other hand, the cooperation between internal collisional processes and external tidal effects will determine a mass loss of the individual infant GC candidates as they orbit around the center of mass of their host galaxy. In addition, stellar evolution will also likely play a significant role. The mean mass we find for our infant GC objects is  $6 \times 10^4$  (i.e., about 10 times smaller than that used in SF09), which would allow for a significant contribution from newly formed GCs and subsequent star formation. In any case, the balance between the latter processes and those leading to mass loss in GC system would

require a dedicated investigation. In summary, the main results of this study can be presented as follows:

- We have conducted an analysis of the demographics and properties of low-mass stellar systems at high redshift, within the numerical framework of the FiBY cosmological simulations. We identified a population of  $f_b = 1$  objects with a relatively low fraction of mass in the form of dark matter, which we identify as infant GC candidates.
- We explored how the stellar half-mass radius, density, metallicity and velocity dispersion vary as a function of the stellar mass for our infant GC candidates. For comparison, we also investigated these properties for other groups of low-mass stellar systems identified in our simulations. We believe the  $f_b = 1$  objects are plausible infant GC candidates as they are characterised, among other properties, by high stellar densities when compared to the general population of substructures identified in our cosmological simulations.
- We fit the redshift-zero globular system mass – halo mass relation and found it provides a reasonable fit to our infant GC objects, indicating that this relation is set at formation. Due to its linearity, we speculate that, as these cluster - galaxy systems evolve, they will move along the GC system mass – halo mass relation and be in good agreement with the present-day observations
- We compared the sizes and masses of the infant GCs we found in FiBY to preliminary high redshift observations of globulars from Vanzella et al. (2017) and Bouwens et al. (2017). In both cases, we found a relatively good agreement. Whilst our infant GC candidates are rather dense objects, they appear to be more extended than typical present-day GCs in the local Universe, consistently with the properties of the infant globulars currently observed at high redshifts.
- We investigated the environments that our infant GC candidates reside in. We found that these objects lie within the DM density peaks for their given parent halo, but they contain a low fraction of energetically bound DM particles. Most of our infant GC systems lie within 1 kpc from the center of their parent galaxy. This suggests that even in their first few Myr of evolution these objects have undergone many interactions.

For the future we envisage two main lines of enquiry. The first involves investigating how the  $f_b = 1$  objects came to be. We will look into their past evolution, star formation history and how the infant GCs and their environments have changed over time until  $z = 6$ . This will be done in order to be able to distinguish a particular formation pathway for infant GCs. The second line of enquiry is concerned with the future evolution of our clusters. These objects have a high gas fraction, therefore we wish to investigate how much of this gas is used in subsequent star formation. As stated previously, our infant GC objects appear to be in close proximity to their parent galaxy. This could have an impact on their subsequent evolution and their survivability. We will utilise N-body simulations to study this. Finally, we would like to see how these objects evolve chemically in order to be able make a phenomenological comparison with observations of the Galactic GC system. This study represents a first step in formulating a deeper understanding of the role of low-mass stellar systems in the rapidly evolving landscape of ‘near-field’ cosmology.

**ACKNOWLEDGEMENTS**

FP would like to thank Sukyoung Yi, Hidenobu Yajima, Makito Abe, Joseph Silk and Eugenio Carretta for their useful discussions on this work. ALV wishes to thank S. Kikuchihara, M. S. Fujii, Y. Hirai, N. Yoshida, A. Renzini, M. Cirasuolo and T. Treu for interesting conversations and acknowledges support from a UKRI Future Leaders Fellowship (MR/S018859/1) and a JSPS International Fellowship with Grand-in-Aid (KAKENHI-18F18787).

**REFERENCES**

- Abel T., Anninos P., Zhang Y., Norman M. L., 1997, *NewA*, 2, 181
- Ashman K. M., Zepf S. E., 1992, *The Astrophysical Journal*, 384
- Bastian N., Lardo C., 2018, *Annual Review of Astronomy and Astrophysics*, 56, 83
- Bate M. R., Bonnell I. A., Bromm V., 2003, *MNRAS*, 339, 577
- Baumgardt H., Cote P., Hilker M., Rejkuba M., Mieske S., Djorgovski S. G., Stetson P., 2009, *MNRAS*, 396, 2051
- Bechtol K., et al., 2015, *ApJ*, 807, 50
- Blumenthal G. R., Faber S. M., Primack J. R., Rees M. J., 1984, *Natur*, 311, 517
- Bouwens R. J., Illingworth G. D., Oesch P. A., Maseda M., Ribeiro B., Setfanon M., Lam D., 2017, eprint arXiv:1711.02090
- Boylan-Kolchin M., 2017, *MNRAS*, 472, 3120
- Boylan-Kolchin M., 2018, *MNRAS*, 479, 332
- Brodie J. P., Huchra J. P., 1991, *ApJ*, 379, 157
- Bromm V., Clarke C. J., 2002, *ApJ*, 566, L1
- Brown T. M., et al., 2014, *ApJ*, 796
- Caffau E., et al., 2011, *Nat*, 477, 67
- Carlberg R. G., 2018, *ApJ*, 861, 69
- Chabrier G., 2003, *PASP*, 115, 763
- Conroy C., Loeb A., Spergel D. N., 2011, *ApJ*, 741, 72
- Côté P., Marzke R. O., West M. J., 1998, *The Astrophysical Journal*, 501, 554
- Creasey P., Sales L. V., Peng E. W., Sameie O., 2019, *MNRAS*, 482, 219
- Cullen F., McLure R. J., Khochfar S., Dunlop J. S., Dalla Vecchia C., 2017, *MNRAS*, 470, 3006
- Cullen F., et al., 2019, *MNRAS*, 487, 2038
- Dalla Vecchia C., Schaye J., 2012, *MNRAS*, 426, 140
- Davis M., Efstathiou G., Frenk C. S., White S. D. M., 1985, *ApJ*, 292, 371
- Davis A. J., Khochfar S., Dalla Vecchia C., 2014, *MNRAS*, 443, 985
- Dolag K., Borgani S., Murante G., Springel V., 2009, *MNRAS*, 399, 497
- Elmegreen D. M., Elmegreen B. G., 2017, *ApJ*, 851, L44
- Elmegreen B. G., Malhorta S., Rhoads J., 2012, *The Astrophysical Journal*, 757
- Elson R., Hut P., Inagaki S., 1987, *ARA&A*, 25, 565
- Ferland G. J., Korista K. T., Verner D. A., Ferguson J. W., Kingdon J. B., Verner E. M., 1998, *PASP*, 110, 761
- Forbes D. A., Bridges T., 2010, *MNRAS*, 404, 1203
- Forbes D. A., Brodie J. P., Grillmair C. J., 1997, *Astronomical Journal*, 113
- Forbes D. A., et al., 2018a, *Proceedings of the Royal Society A*, 474
- Forbes D. A., Read J. I., Gieles M., Collins M. L. M., 2018b, *MNRAS*, 481, 5592
- Frebel A., Johnson J. L., Bromm V., 2007, *MNRAS*, 380, L40
- Gaia Collaboration et al., 2018, *A&A*, 616, A12
- Galli D., Palla F., 1998, *A&A*, 335, 403
- Gratton R. G., Carretta E., Bragaglia A., 2012, *A&ARv*, 20, 50
- Halbesma T. L. R., Grand R. J. J., Gomez F. A., Marinacci F., Pakmor R., Trick W. H., Busch P., White S. D. M., 2019, arXiv, p. 1909.02630
- Harris W. E., 1991, *ARA&A*, 29, 543
- Harris W. E., 1996, *Astronomical Journal*, 112, 1487
- Harris W. E., 2016, *AJ*, 151
- Harris W. E., Racine R., 1979, *ARA&A*, 17, 241
- Harris W. E., Harris G. L. H., Alessi M., 2013, *The Astrophysical Journal*, 772
- Harris W. E., Harris G. L., Hudson M. J., 2015, *The Astrophysical Journal*, 806
- Harris W. E., Blakeslee J. P., Harris G. L., 2017, *The Astrophysical Journal*, 836
- Heggie D. C., Hut P., 1996, *IAUS*, 174, 303
- Heggie D., Hut P., 2003, Cambridge University Press, p. 372
- Hirschmann M., Khochfar S., Burkert A., Naab T., Genel S., Somerville R. S., 2010, *MNRAS*, 407, 1016
- Hudson M. J., Harris G. L., Harris W. E., 2014, *ApJL*, 787, L5
- Hurst T. J., Zentner A. R., 2019, arXiv, 1910, 00665
- Ibata R., Nipoti C., Sollima A., Bellazzini M., Chapman S. C., Dalessandro E., 2013, *MNRAS*, 428, 3648
- Ishiyama T., et al., 2013, *ApJ*, 767, 146
- Jahnke K., Macciò A. V., 2011, *ApJ*, 734
- Johnson J. L., Dalla Vecchia C., Khochfar S., 2013, *MNRAS*, 428, 1857
- Kaiser N., 1984, *ApJL*, 284, L9
- Katz H., Ricotti M., 2013, *MNRAS*, 432, 3250
- Katz H., Ricotti M., 2014, *MNRAS*, 444, 2377
- Kennicutt R. C. J., 1998, *ARA&A*, 36, 189
- Kikuchihara S., Ouchi M., et al., 2019, arXiv, 1905, 06927
- Kim J., et al., 2018, *MNRAS*, 474, 4232
- Komatsu E., et al., 2011, *ApJS*, 192
- Koposov S. E., Belokurov V., Torrealba G., Evans N. W., 2015, *ApJ*, 805, 130
- Kravtsov A. V., Gnedin O. Y., 2005, *ApJ*, 623, 650
- Kruijssen J. M. D., 2014, *CQGra*, 31, 244006
- Kruijssen J. M. D., 2015, *MNRAS*, 454, 1658
- Kruijssen J. M. D., Pfeffer J. L., Reina-Campos M., Crain R. A., Bastian N., 2019, *MNRAS*, 486, 3180
- Lane R. R., et al., 2010, *MNRAS*, 406, 2732
- Lardo C., Bellazzini M., Pancino E., Carretta E., Bragaglia A., Dalessandro E., 2011, *Astronomy and Astrophysics*, 525
- Larsen S. S., Brodie J. P., Huchra J. P., Forbes D. A., Grillmair C. J., 2001, *The Astronomical Journal*, 121, 2974
- Larsen S. S., Brodie J. P., Sarajedini A., Huchra J. P., 2002, *AJ*, 124, 2615
- Leaman R., VandenBerg D. A., Mendel J. T., 2013, *MNRAS*, 436, 122
- Li H., Gnedin O. Y., 2019, *MNRAS*, 486, 4030
- Ma X., et al., 2019, eprint arXiv:1906.11261
- Maio U., Khochfar S., Johnson J. L., Ciardi B., 2011, *MNRAS*, 414, 1145
- Mashchenko S., Sills A., 2005, *ApJ*, 619, 243
- Masters K. L., et al., 2010, *ApJ*, 715, 1419
- McLaughlin D. E., van der Marel R. P., 2005, *The Astrophysical Journal Supplement Series*, 161, 304
- Meylan G., Heggie D. C., 1997, *A&ARv*, 8, 1
- Milone A. P., et al., 2017, *MNRAS*, 464, 3636
- Moore B., 1996, *ApJ*, 461, L13
- Muratov A. L., Gnedin O. Y., 2010, *ApJ*, 718, 1266
- Nakasato N., Mori M., Nomoto K., 2000, *ApJ*, 535, 776
- Neistein E. L. C., Khochfar S., Weinmann S. M., Shankar F., Boylan-Kolchin M., 2011, *MNRAS*, 416, 1486
- Paardekooper J. P., Khochfar S., Dalla C. V., 2013, *MNRAS*, 429, L94
- Paardekooper J. P., Khochfar S., Dalla Vecchia C., 2015, *MNRAS*, 451, 2544



- Peebles P. J. E., 1984, *ApJ*, 277, 470
- Peebles P. J. E., Dicke R. H., 1968, *The Astrophysical Journal*, 154
- Penarrubia J., Varri A. L., Breen P. G., Ferguson A. M. N., Sanchez-Janssen R., 2017, *MNRAS*, 471, L31
- Peng E. W., et al., 2006, *The Astrophysical Journal*, 639, 95
- Piotto G., et al., 2015, *The Astronomical Journal*, 149
- Pontzen A., Governato F., 2012, *MNRAS*, 421, 3464
- Portegies Zwart S. F., McMillan S. L. W., 2000, *The Astrophysical Journal*, 528, L17
- Portegies Zwart S. F., McMillan S. L. W., Gieles M., 2010, *ARA&A*, 48, 431
- Pozzetti L., Maraston C., Renzini A., 2019, *MNRAS*, 485, 5861
- Prieto J. L., Gnedin O. Y., 2008, *ApJ*, 689, 919
- Recio-Blanco A., 2018, *Astronomy & Astrophysics*, 620
- Reina-Campos M., Kruijssen J. M. D., Pfeffer J. L., Bastian N., Crain R. A., 2019, *MNRAS*, 486, 5838
- Renaud F., 2018, *New Astronomy Reviews*, 81, 1
- Renaud F., Agertz O., Gieles M., 2017, *MNRAS*, 465, 3622
- Renzini A., 2017, *MNRAS*, 469, L63
- Ricotti M., 2002, *MNRAS*, 336, L33
- Ricotti M., Parry O. H., Gnedin N. Y., 2016, *The Astrophysical Journal*, 831
- Rieder S., Ishiyama T., Langelaan P., Makino J., McMillan S. L. W., Portegies Zwart S., 2013, *MNRAS*, 436, 3695
- Rodriguez C. L., Morscher M., Pattabiraman B., Chatterjee S., Haster C. J., Rasio F. A., 2015, *Physical Review Letters*, 115
- Rosenblatt E. I., Faber S. M., Blumenthal G. R., 1988, *ApJ*, 330, 191
- Saitoh T. R., Koda J., Okamoto T., Wada K., Habe A., 2006, *ApJ*, 640, 22
- Salpeter E. E., 1955, *ApJ*, 121, 161
- Schaye J., Dalla Vecchia C., 2008, *MNRAS*, 383, 1210
- Schaye J., et al., 2010, *MNRAS*, 402, 1536
- Schmidt M., 1959, *ApJ*, 129, 243
- Schweizer F., 1987, *Nearly Normal Galaxies. From the Planck Times to the Present. The Eighth Santa Cruz Summer Workshop in Astronomy and Astrophysics*
- Simon J. D., 2019, *ARA&A*, 57, 375
- Simon J. D., et al., 2015, *ApJ*, 808, 95
- Spitler L. R., Forbes D. A., 2009, *MNRAS*, 392, L1
- Springel V., 2005, *MNRAS*, 364, 1105
- Springel V., Yoshida N., White S. D. M., 2001, *New Astronomy*, 6, 79
- Springel V., et al., 2005, *Natur*, 435, 629
- Tonini C., 2013, *The Astrophysical Journal*, 762
- Vanzella E., et al., 2017, *MNRAS*, 467, 4304
- Vanzella E., et al., 2019, *MNRAS*, 483, 3618
- Westmeier T., Staveley-Smith L., Calabretta M., Jurek R., Koribalski B. S., Meyer M., Popping A., Wong O. I., 2015, *MNRAS*, 453, 338
- Wiersma R. P. C., Schaye J., Smith B. D., 2009, *MNRAS*, 393, 99
- Yoshida N., Omukai K., Hernquist L., Abel T., 2006, *ApJ*, 652, 6
- van den Bergh S., 2000, *PASP*, 112, 932

This paper has been typeset from a  $\text{\TeX}/\text{\LaTeX}$  file prepared by the author.